metals

MDPI

Article

Mechanical Amorphization and Recrystallization of Mn-Co(Fe)-Ge(Si) Compositions

Antonio Vidal-Crespo, Jhon J. Ipus, Javier S. Blázquez * and Alejandro Conde

Departamento Física de la Materia Condensada, ICMSE-CSIC, Universidad de Sevilla, 41080 Sevilla, Spain; antvidcre@alum.us.es (A.V.-C.); jhonipus@us.es (J.J.I.); conde@us.es (A.C.)

* Correspondence: jsebas@us.es; Tel.: +34-954-556-029

Received: 18 April 2019; Accepted: 6 May 2019; Published: 8 May 2019

Abstract: Mechanical alloying using a planetary ball mill allowed us to obtain two homogeneous systems formed by units with nanometer size and $MnCo_{0.8}Fe_{0.2}Ge_{1-x}Si_x$ stoichiometry (x = 0 and 0.5). The phase evolution of the systems with the milling time was analyzed using X-ray diffraction. Thermal stability of the final products was studied using differential scanning calorimetry. Room temperature ^{57}Fe Mössbauer spectroscopy was used to follow the changes in the Fe environments. A paramagnetic Co-based amorphous phase developed in both alloys as milling progressed. However, while the presence of Si stabilized the Mn-type phase, mechanical recrystallization was observed in a Si-free composition leading to the formation of a MnCo(Fe)Ge intermetallic (*Pnma* space group) with a crystal size of 7 ± 1 nm. Mössbauer results indicate that Fe atoms migrate from the initial bcc phase to the amorphous and intermetallic phases.

Keywords: half-Heusler alloys; mechanical alloying; Mössbauer spectroscopy

1. Introduction

Half-Heusler MnCoGe alloys can show a martensitic transformation from an orthorhombic TiNiSi-type structure (*Pnma* space group) to a hexagonal Ni_2In-type structure ($P6_3/mmc$, although it can be also interpreted as a different orthorrombic *Pnma* structure with different lattice parameters to those of the TiNiSi-type structure [1]). Coincidence of such a structural transformation with a magnetic one has been proposed to enhance the magnetocaloric effect exhibited by these systems [2], which can be achieved by compositional tailoring with partial substitution of Fe for Co [3]. However, the formation of the intermetallic phase of interest is not straightforward and long-duration annealing at high temperatures is needed (typically several days at ~1125 K [3–5]).

On the other hand, high entropy alloys (HEAs) are homogeneous solid solutions formed by at least five different elements with atomic fractions between 5 and 35 at. % [6]. In such HEAs, bcc and fcc solid solutions as well as amorphous phases can be observed as product phases when produced by rapid quenching [7] or mechanical alloying [8]. Both amorphous and supersaturated solid solutions are very attractive homogeneous precursor systems to develop stoichiometric intermetallic phases, strongly reducing the annealing time required with respect to the samples obtained by conventional methods [9]. The development of HEAs from half-Heusler compositions has been recently reported for Ti(NiCo)(SnSb) [10], CoMnSn(Cu) [11] and (TiZr)Ni(SnSb) [12] systems.

The aim of this study is to produce homogeneous systems starting from pure powders with $MnCo_{0.8}Fe_{0.2}Ge_{1-x}Si_x$ stoichiometry (with x = 0 and x = 0.5) using mechanical alloying.

2. Materials and Methods

Pure Mn (99.6%, Alfa Aesar, Karlsruhe, Germany), Co (99.99%, Chempur, Karlsruhe, Germany), Ge (99.99%, Chempur, Karlsruhe, Germany), Si (99.9%, Alfa Aesar, Karlsruhe, Germany) and Fe (>99%,

Alfa Aesar, Karlsruhe, Germany) powders (5 g) were mixed in hardened steel vials with 10 mm steel balls in an argon atmosphere and ball milled up to 100 h at 250 rpm in a Pulverisette Vario 4 mill (Fritsch, Idar-Oberstein, Germany) with a frequency ratio of −2 and a ball mass to powder ratio, BPR = 10. Compositions were checked using EAGLE III (EDAX, Mahwah, NJ, USA) X-ray microfluorescence equipment. X-ray diffraction (XRD) experiments were performed using a powder diffractometer D8 Advance A25 (Bruker, Karlsruhe, Germany) at room temperature and the radiation employed was Cu K_α. Experimental patterns were fitted using TOPAS software (Version 6, Bruker, Karlsruhe, Germany). No preferential orientation was allowed to preserve the intensity ratio in our powder samples. Transmission ^{57}Fe Mössbauer (MS) spectra at room temperature were obtained using a Wissel spectrometer (Wissel, Starnberg, Germany). Isomer shifts were measured relative to that of a standard foil of pure Fe. Differential scanning calorimetry (DSC) experiments were performed using a DSC7 (Perkin-Elmer, Norwalk, CT, USA) calorimeter at a heating rate of 20 K/min.

3. Results

3.1. X-ray Diffraction

Figure 1 shows the evolution of the XRD patterns as a function of the milling time. These patterns can be fitted using the Rietveld method assuming the different starting pure phases, except for Si (the lightest among the studied elements), which is not detected even after 1 h milling, indicating its integration to the other phases. Table 1 shows the R-factors of the different fittings and Table 2 shows the lattice parameter of the different phases detected. The diffraction maxima of the starting hcp Co phase rapidly broadens beyond any realistic values of crystal size or microstrains, which is due to the formation of an amorphous phase in both compositions. In order to account for this amorphous phase, we allowed the amorphous halo associated to this phase to evolve directly from the diffraction maxima of the hcp Co phase. Although Rietveld fitting of an amorphous phase could lead to unphysical results of the parameters (e.g., extremely low crystal size or extremely high microstrains), our aim was just to estimate the phase fraction evolution along the milling.

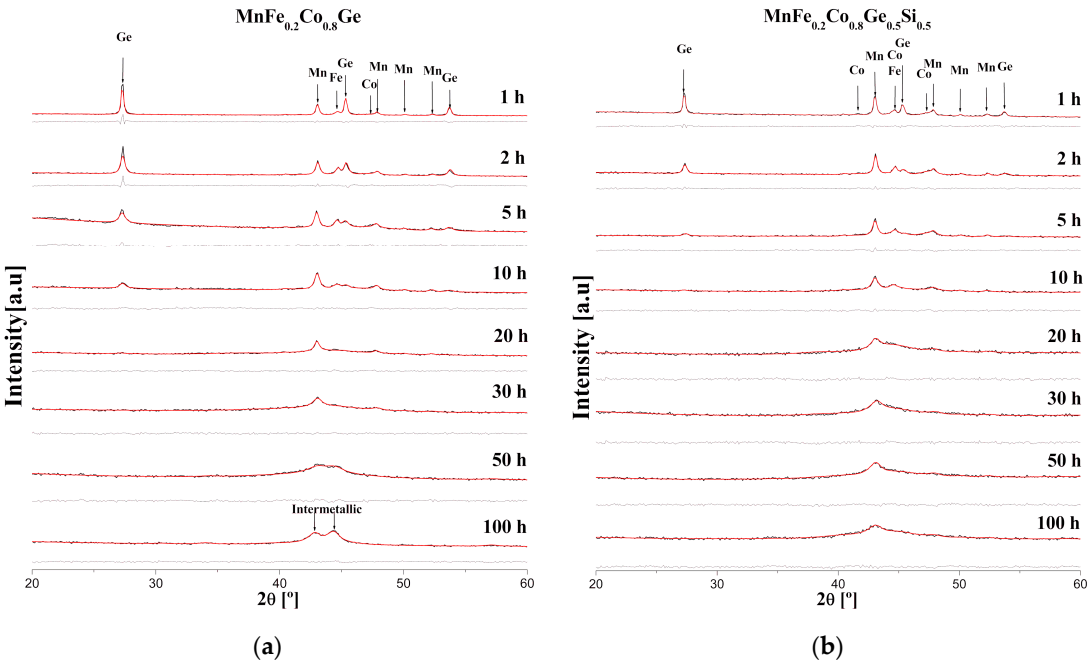

Figure 1. X-ray diffraction (XRD) patterns of samples after different times of milling: (**a**) Si-free alloy (**b**) Si-containing alloy. The corresponding differences between the experimental data and the Rietveld fittings are shown below each experimental pattern. The experimental data in black and the fitting in red.

Rietveld fitting (see R-values in Table 1 for each pattern) supplies valuable information concerning phase fraction, lattice parameter, crystal size and microstrains. In the following we will account only for the crystal size as the main factor for peak broadening (i.e., a minimum crystal size is reported). Figure 2 shows the phase fraction evolution with the milling time of the two studied compositions and Figure 3 shows the corresponding crystal size.

Table 1. Parameters from Rietveld fittings.

Si-Free Alloy				Si-Containing Alloy			
Milling Time (h)	R_{exp}	R_{wp}	χ^2	**Milling Time (h)**	R_{exp}	R_{wp}	χ^2
1	2.20	3.87	1.76	1	2.36	2.90	1.23
2	2.23	3.37	1.51	2	2.33	2.61	1.12
5	2.29	2.98	1.30	5	2.17	2.44	1.12
10	2.24	2.60	1.16	10	2.26	2.39	1.06
20	2.01	2.07	1.03	20	2.21	2.59	1.17
30	2.01	2.08	1.07	30	2.21	2.54	1.15
50	2.02	2.36	1.17	50	2.22	2.31	1.04
100	2.07	2.28	1.10	100	2.08	2.28	1.10
Crystalline	2.16	3.08	1.43	Crystalline	2.22	3.37	1.52

Table 2. Average lattice parameters of the crystalline phases detected by XRD. Changes in this parameter with the milling time is of the order of the error bar.

Phase	**Space Group**	**Lattice Parameter (Å)**	
		Si-Free	**Si-Containing**
Mn	*I4-3m*	8.916 ± 0.003	8.893 ± 0.009
Ge	*Fd-3m*	5.656 ± 0.002	5.656 ± 0.006
Fe(Co)	*Im-3m*	2.870 ± 0.002	2.870 ± 0.002
MnCo(Fe)Ge	*Pnma*	a = 5.20 ± 0.02 b = 4.15 ± 0.04 c = 7.0 ± 0.2	-
MnCo(Fe)Ge *	*Pnma*	a = 5.2822 ± 0.0002 b = 4.0750 ± 0.0003 c = 7.0440 ± 0.0005	-
Bcc solid solution *	*Im-3m*	-	2.8835 ± 0.0001

* Samples heated up to 973 K at 20 K/min in argon flow.

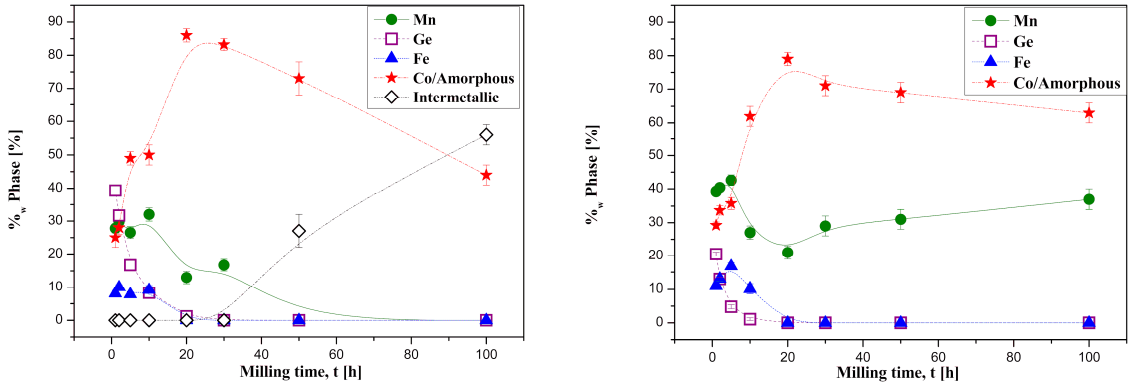

Figure 2. Phase fraction from XRD Rietveld analysis as a function of the milling time: (**a**) Si-free alloy (**b**) Si-containing alloy. Lines are a guide to the eye.

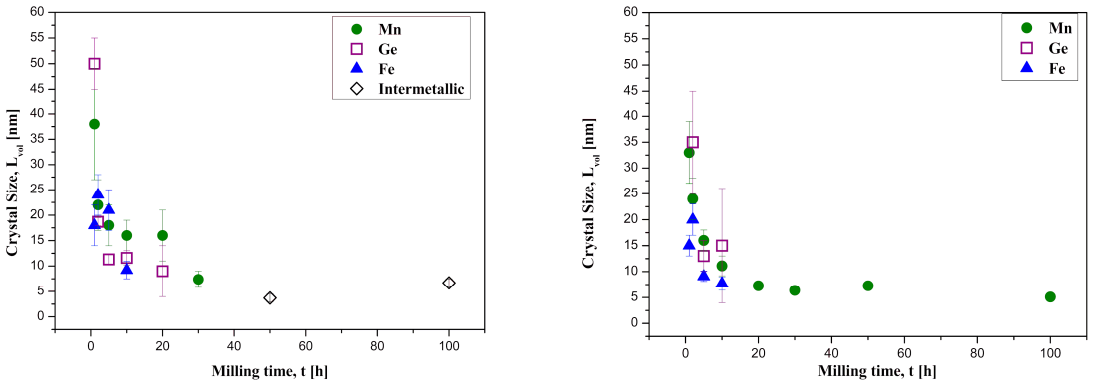

Figure 3. Crystal size from XRD Rietveld analysis as a function of the milling time: (**a**) Si-free alloy (**b**) Si-containing alloy.

The fraction of the diamond-like Ge phase (*Fd-3m* space group) exponentially decreased with milling time for both studied compositions. The content of bcc-Fe-type phase (*Im-3m* space group) initially reached values above the starting weight fraction of Fe, indicating the migration of other atoms (mainly Co and Si) to this phase. After 10 h of milling, the decrease of the weight fraction for this phase was clear and was no longer detected by XRD after 20 h milling. The evolution of the Mn phase fraction depends on the Si content of the sample. Whereas for Si-free alloy, the Mn-type phase was no longer detected by XRD after 50 h milling; for Si-containing alloy, the Mn-type phase remained almost constant (or even increased) from 10 h up to the maximum time explored in this study (100 h).

As written above, Rietveld fitting showed that the crystal size of the Co-type phase ($P6_3/mmc$ space group) rapidly decreased with milling time (below 2 nm after 5 h milling for Si-free alloy and after 10 h milling for Si-containing alloy). Therefore, the diffraction maxima ascribed to this phase no longer describe a crystalline phase but rather amorphous halos ascribed to an amorphous phase. The distinction between crystalline Co-type and Co-base amorphous phase is not clear. Therefore, the two phases are represented together in Figure 2.

Lattice parameters did not change significantly with the milling time but the average values could differ with respect to the values of the pure phases. This should indicate that e.g., Co migration to bcc Fe occurs at the early stages of milling, in agreement with the higher fraction measured for this phase (8–10 wt. %) with respect to the nominal Fe fraction (6.0 and 6.8 wt. % for the alloys without and with Si). In the case of Ge, the measured lattice parameter agreed with that of the pure phase, indicating that this element preserves its purity during its comminution. In the case of the Mn phase, the presence of Si stabilizes it and reduces the lattice parameter with respect to that of the Si-free composition. Average values of lattice parameters of the different phases are shown in Table 2.

3.2. Mössbauer Spectroscopy

Figure 4 shows the evolution of the Mössbauer spectra with the milling time. Two main contributions can be clearly distinguished: a ferromagnetic contribution (FM) and a paramagnetic (PM) one. The FM contribution corresponds to Fe atoms in the bcc Fe(Co) phase as it is confirmed by the hyperfine field HF~33 T. This may indicate that Fe content in crystalline hcp Co at the early stages is negligible (no site is detected). As milling time increased, FM contribution reduced to zero at around 20 h milling, whereas the PM contribution was present since the earlier studied times and progressively increased with milling. Therefore, as the FM contribution is clearly assigned to bcc-Fe type sites, the rest of the phases, which contain Fe, detected by XRD, must be paramagnetic, including the amorphous phase derived from broadening of the hcp-Co diffraction maxima.

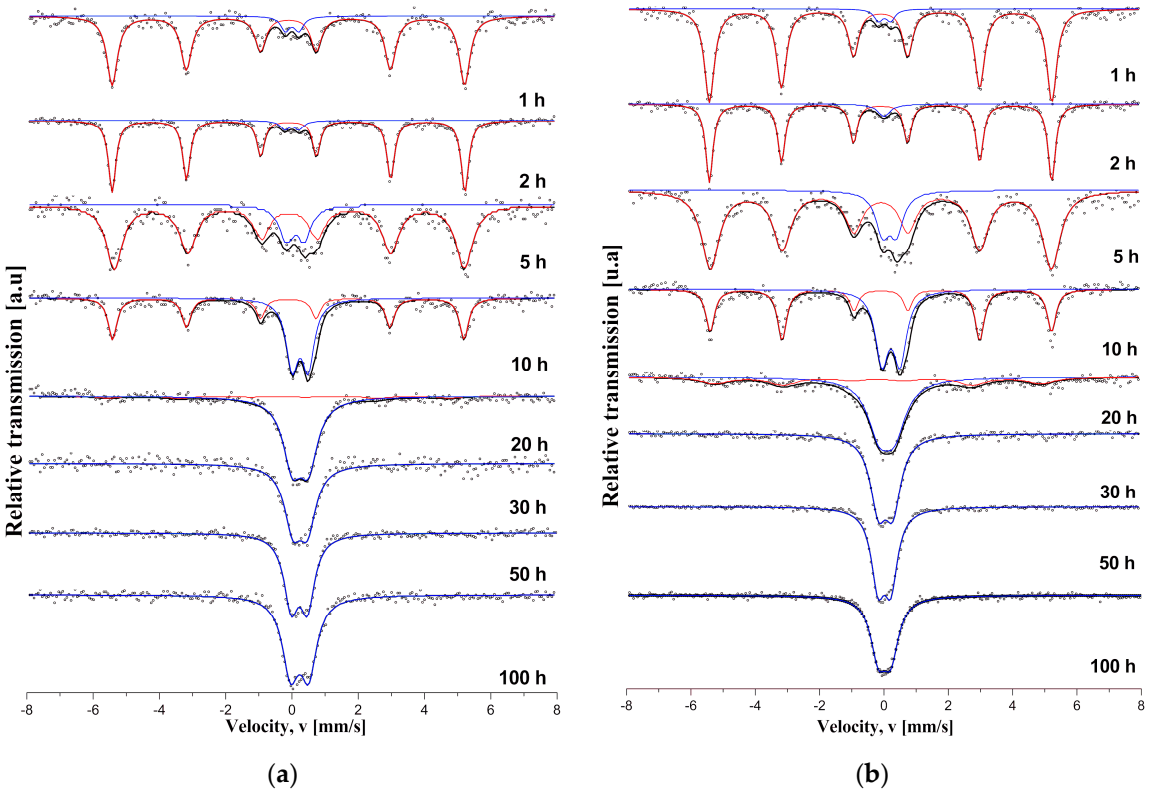

Figure 4. Room temperature Mössbauer spectra as a function of the milling time of: (**a**) Si-free alloy and (**b**) Si-containing alloy samples.

4. Discussion

The recrystallization process was detected only in Si-free alloys, leading to the formation of an intermetallic phase: MnCo(Fe)Ge (*Pnma* space group), with a crystal size <10 nm for as-milled samples after 50 and 100 h (see Figure 3a). The presence of the recrystallization phenomenon was confirmed by DSC. Figure 5a shows the DSC scan of Si-free samples milled for 50 h and 100 h, respectively. The transformation heat, $|\Delta H|$, of the exothermic peak at ~550 K strongly decreased from the sample milled for 50 h to the sample milled for 100 h (from $\Delta H = -38$ to -16 ± 1 J/g, while the amorphous fraction from XRD decreased from 73 to 44%) due to the recrystallization phenomenon. In fact, XRD patterns of samples heated above the exothermic peak showed the intermetallic MnCoGe-type phase as the single phase present except for some traces of MnO (as shown in Figure 6).

In the case of the Si-containing sample after 100 h milling, DSC of Figure 5b shows a minor exothermic peak at ~550 K but the main transformation peak is found at ~620 K ($\Delta H = -114 \pm 1$ J/g). Samples heated above this temperature transformed to a single bcc solid solution. At higher temperatures, ~850 K, an endothermic and reversible peak was found.

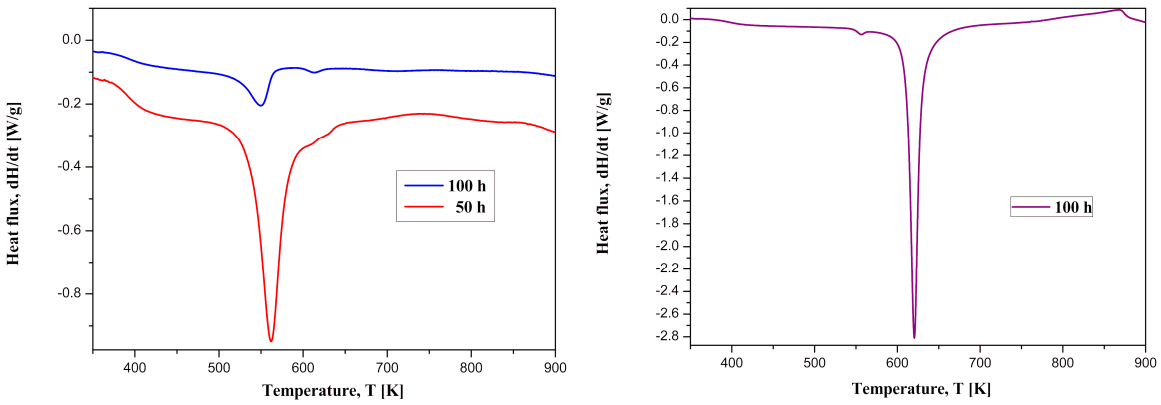

Figure 5. DSC scans at 20 K/min for: (**a**) Si-free alloy after 50 and 100 h milling (**b**) Si-containing alloy after 100 h milling.

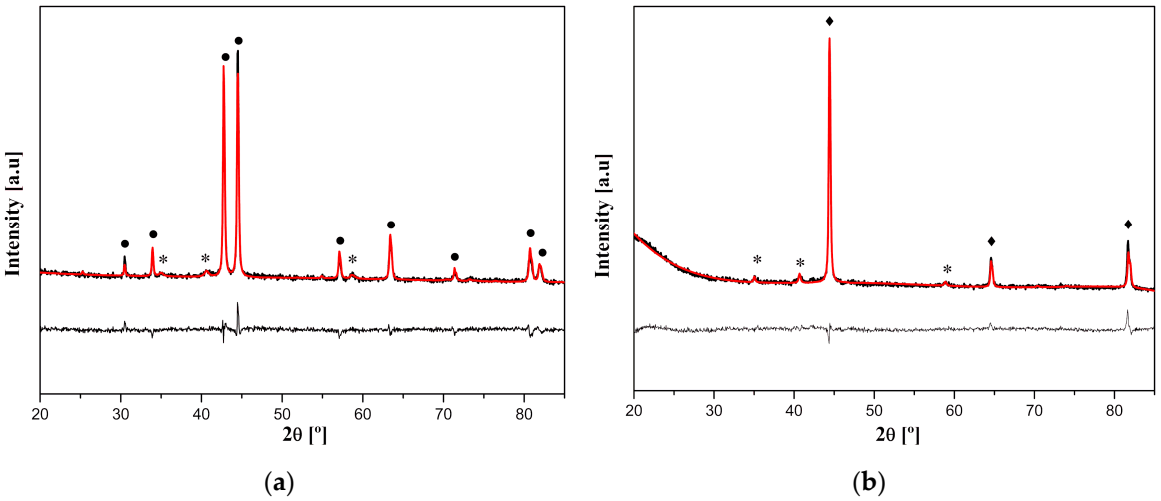

Figure 6. XRD patterns of samples milled for 100 h and heated up to 973 K at 20 K/min: (**a**) Si-free alloy (**b**) Si-containing alloy. Circles identify intermetallic phase, diamonds identify bcc solid solution and asterisks identify MnO phase. The experimental data are in black and the fitting in red. Corresponding differences between the experimental and fitting curves are shown below each experimental pattern.

The formation of such simple structures in Si-containing alloy (amorphous and bcc solid solution) is typically found in HEA. These systems can be characterized by several parameters:

Mixing enthalpy, ΔH_{mix};

$$\Delta H_{mix} = 4 \sum_{i,j<i} c_i c_j \Delta H_{mix}^{ij}, \quad (1)$$

with c_i the molar fraction of the i element in the composition and ΔH_{mix}^{ij}, the mixing enthalpy between the elements i and j. For non-metals such as Si and Ge, it is necessary to calibrate ΔH_{mix}^{ij} to subtract the extra energy, ΔH^{trans}, required to transform the element from non-metallic to metallic and: $\Delta H_{mix}^{ij*} = \Delta H_{mix}^{ij} - \Delta H^{trans}/2$. For Si and Ge, ΔH^{trans} of 34 or 25 kJ/mol [13], respectively.

Atomic-size difference, δ:

$$\delta = \sqrt{\sum_{i=1}^{N} c_i \left(1 - \frac{r_i}{\sum_{i=1}^{N} c_i r_i}\right)^2}, \quad (2)$$

where r_i is the atomic radius of the i element. And Ω parameter:

$$\Omega = \frac{T_m \Delta S_{mix}}{\Delta H_{mix}}, \quad (3)$$

where T_m is the weighted average of the melting temperature of the composition and

$$\Delta S_{mix} = -R \sum_i c_i ln(c_i), \quad (4)$$

Taking the values of r_i and ΔH_{mix}^{ij} from [6,13], the results for the quinary composition are ΔH_{mix} = −33 kJ/mol, δ = 5.4% and Ω = 0.60. While the quaternary composition has ΔH_{mix} = −25 kJ/mol, δ = 3.9% and Ω = 0.64. These parameters place our studied alloys close to the bulk amorphous region of HEA depicted in [6]. This could agree with the easy formation of the amorphous phase in our studied samples. However, although the studied quinary composition develops a single bcc phase solid solution after thermal treatment, HEA with such solid solution generally shows larger Ω and less negative ΔH_{mix} [6].

Despite the low content of Fe in the studied compositions (~6.7 at. %), MS can supply some information to confirm the evolution of the phases during milling. As already described, the only FM site detected corresponds to the bcc-Fe(Co) phase and was fitted using a broad sextet centered at HF~33 T, which confirms the rapid transformation of the FM hcp-Co phase to a PM Co-based amorphous phase enriched in Ge and Mn (or at least the negligible Fe content in the residual hcp-Co phase).

The PM contribution was fitted using a doublet with quadrupolar splitting, <Q> = 0.48 ± 0.07 mm/s (Si-free alloy) and 0.42 ± 0.15 mm/s (Si-containing alloy). In the case of Si-free alloy, both Q and IS remain almost constant along the milling process indicating that the Fe sites out of the bcc phase might be similar (i.e., Fe atoms are not expected to migrate to many different phases). In the case of Si-containing alloy, whereas Q is almost constant, IS becomes more positive as milling time increases. A clear correlation can be observed between the area fraction of the PM contribution and the amorphous fraction measured from XRD for both compositions up to 30 and 20 h of milling for Si-free and Si-containing alloy, respectively. Figure 7 shows this correlation. In the case of Si-free alloy, correlation is preserved for all times when amorphous and intermetallic phase fractions are considered. This indicates that Fe atoms migrate to these two phases in Si-free alloy.

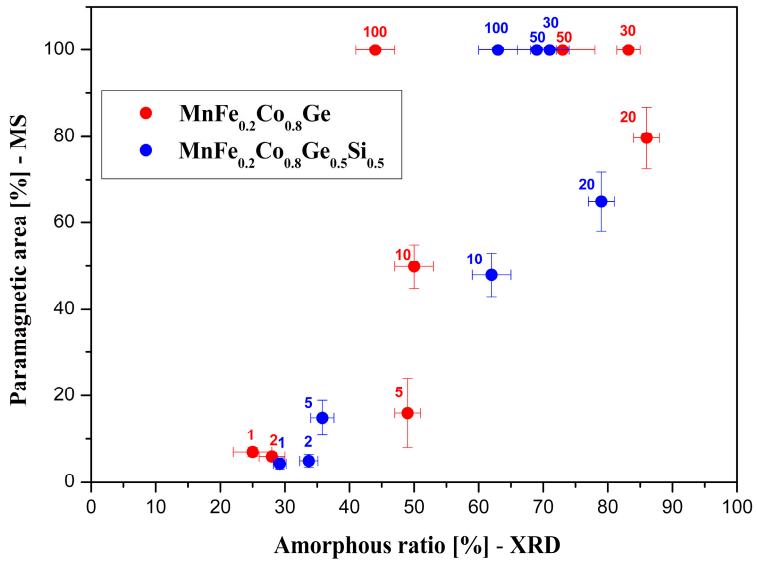

Figure 7. Amorphous fraction from XRD Rietveld analysis as a function of PM contribution from MS for Si-free alloy (in red) and Si-containing alloy (in blue). Numbers indicate the milling time in hours for each composition.

5. Conclusions

Two different compositions $MnCo_{0.8}Fe_{0.2}(Ge_{1-x}Si_x)$ were partially amorphized by mechanical alloying. X-ray diffraction and Mössbauer spectrometry were used to characterize the evolution of the different phases with milling time.

In the case of the Si-free alloy, almost fully amorphization was achieved after 50 h milling, and further milling led to the development of MnCoGe-type intermetallic. Thermal treatment beyond ~650 K led to the growth of this intermetallic, and the alloy became single phase.

In the case of the Si-containing alloy, the Mn-phase fraction remained almost constant from 30 to 100 h milling and the alloy became only partially amorphous during milling. Thermal treatment beyond ~650 K led to the formation of a bcc solid solution, which is characteristic for high entropy alloys.

Author Contributions: Conceptualization of the project: A.V.-C., J.J.I., J.S.B. and A.C. Discussion of the results and revision of the paper: A.V.-C., J.J.I., J.S.B. and A.C. Experiments were developed by A.V.-C., J.J.I., and J.S.B.

Funding: This research was funded by AEI/FEDER-UE (Project MAT 2016-77265-R) and the PAI of the Regional Government of Andalucía.

Conflicts of Interest: The authors declare no conflict of interest.

References

1. Jeitschko, W. A High-Temperature X-ray Study of the Displacive Phase Transition in MnCoGe. *Acta Crystallogr. Sect. B: Struct. Sci.* **1975**, *31*, 1187–1190. [CrossRef]
2. Johnson, V. Diffusionless orthorhombic to hexagonal transitions in ternary silicides and germanides. *Inorg. Chem.* **1975**, *14*, 1117–1120. [CrossRef]
3. Li, G.; Liu, E.; Zhang, H.; Zhang, Y.; Chen, J.; Wang, W.; Zhang, H.; Wu, H.; Yu, H. Phase diagram, ferromagnetic martensitic transformation and magnetoresponsive properties of Fe-doped MnCoGe alloys. *J. Magn. Magn. Mater.* **2013**, *332*, 146–150. [CrossRef]
4. Ozono, K.; Mitsui, Y.; Umetsu, R.; Hiroi, M.; Takahashi, K.; Koyama, K. Magnetic and structural properties of MnCo1-xFexGe (0 ≤ x ≤ 0.12). *AIP Conf. Proc.* **2016**, *1763*. [CrossRef]
5. Lin, S.; Tegus, O.; Bruck, E.; Dagula, W.; Gortenmulder, T.; Buschow, K. Structural and Magnetic Properties of $MnFe_1$-xCoxGe Compounds. *IEEE Trans. Mag.* **2006**, *42*, 3776–3778. [CrossRef]
6. Zhang, Y.; Zuo, T.; Tang, Z.; Gao, M.; Dahmen, K.; Liaw, P.; Lu, Z. Microstructures and properties of high-entropy alloys. *Prog. Mater. Sci.* **2014**, *61*, 1–93. [CrossRef]

7. Singh, S.; Wanderka, N.; Murty, B.; Glatzel, U.; Banhart, J. Decomposition in multi-component AlCoCrCuFeNi high-entropy alloy. *Acta Mater.* **2011**, *59*, 182–190. [CrossRef]
8. Chen, Y.; Tsai, C.; Juan, C.; Chuang, M.; Yeh, J.; Chin, T.; Chen, S. Amorphization of equimolar alloys with HCP elements during mechanical alloying. *J. Alloys Compd.* **2010**, *506*, 210–215. [CrossRef]
9. Blázquez, J.S.; Ipus, J.J.; Moreno-Ramírez, L.M.; Álvarez-Gómez, J.M.; Sánchez-Jiménez, D.; Lozano-Pérez, S.; Franco, V.; Conde, A. Ball milling as a way to produce magnetic and magnetocaloric materials: A review. *J. Mater. Sci.* **2017**, *52*, 11834–11850. [CrossRef]
10. Karati, A.; Nagini, M.; Ghosh, S.; Shabadi, R.; Pradeep, K.G.; Mallik, R.C.; Murty, B.S.; Varadaraju, U.V. Ti_2NiCoSnSb—A new halfHeusler type high-entropy alloy showing simultaneous increase in Seebeck coefcient and electrical conductivity for thermoelectric applications. *Sci. Rep.* **2019**, *9*, 5331. [CrossRef]
11. Guo, Z.; Qiu, H.; Liu, Z. Effects of the substitution of Cu for Sn on structural, magnetic andmagnetocaloric properties of half-Heusler CoMnSn alloy. *J. Alloys Compd.* **2019**, *777*, 472–477. [CrossRef]
12. Rogl, G.; Yubuta, K.; Romaka, V.V.; Michor, H.; Schafler, E.; Grytsiv, A.; Bauer, E.; Rogl, P. High-ZT half-Heusler thermoelectrics, $Ti_{0.5}Zr_{0.5}$NiSn and $Ti_{0.5}Zr_{0.5}NiSn_{0.98}Sb_{0.02}$: Physical properties at low temperatures. *Acta Mater.* **2019**, *166*, 466–483. [CrossRef]
13. Takeuchi, A.; Inoue, A. Calculations of Mixing Enthalpy and Mismatch Entropy for Ternary Amorphous Alloys. *Mater. Trans. JIM* **2000**, *41*, 1372–1378. [CrossRef]

© 2019 by the authors. Licensee MDPI, Basel, Switzerland. This article is an open access article distributed under the terms and conditions of the Creative Commons Attribution (CC BY) license (http://creativecommons.org/licenses/by/4.0/).